FERMILAB-PUB-15-555
ACCEPTED

Methodology for the neutron time of flight measurement of 120-GeV proton-induced reactions on a thick copper target

T. Sanami*[a], Y. Iwamoto[b], T. Kajimoto[c], N. Shigyo[c], M. Hagiwara[a], H.S. Lee[d], E. Ramberg[e], R. Coleman[e], A. Soha[e], D. Jensen[e], A. Leveling[e], N.V. Mokhov[e], D. Boehnlein[e], K. Vaziri[e], K. Ishibashi[c], Y. Sakamoto[b], H. Nakashima[b]

[a]*High Energy Accelerator Research Organization, Oho, Tsukuba, 305-0801 Japan*

[b]*Japan Atomic Energy Agency, Tokai, Ibaraki, 319-1195 Japan*

[c]*Kyushu University, Motooka, Fukuoka, 819-0395 Japan*

[d]*Pohang Accelerator Laboratory, POSTECH, Pohang, Kyungbuk 790-784, Korea*

[e]*Fermi National Accelerator Laboratory, Batavia, IL 60510-5011 USA*

Submitted to Nuclear Instruments and Methods for Physics Research, Section A

Operated by Fermi Research Alliance, LLC under Contract No. De-AC02-07CH11359 with the United States Department of Energy.

Abstract

A methodology for the time-of-flight measurement of the neutron energy spectrum for a high-energy proton-beam-induced reaction was established at the Fermilab Test Beam Facility of the Fermi National Accelerator Laboratory. The 120-GeV proton beam with 3×10^5 protons/spill was prepared for event-by-event counting of incident protons and emitted neutrons for time-of-flight energy determination. An NE213 organic liquid scintillator (12.7 cm in diameter by 12.7 cm in length) was employed with a veto plastic scintillator and a pulse-shape discrimination technique to identify neutrons. Raw waveforms of NE213, veto and beam detectors were recorded to discriminate the effects of multi-proton beam events by considering different time windows. The neutron energy spectrum ranging from 10 to 800 MeV was obtained for a 60-cm-long copper target at 90 degrees with respect to the beam axis. The obtained spectrum was consistent with that deduced employing the conventional unfolding technique as well as that obtained in a 40-GeV/c thin-target experiment.

Keywords: Neutron spectrum, Time-of-flight method, 120-GeV proton, Copper target, NE213 liquid scintillator

1. Introduction

Neutron data are an important parameter for the radiation safety design of high-energy accelerators since many neutrons are produced when beam particles hit a beam pipe, collimator, target or beam dump. For high-energy accelerators, neutrons frequently dominate the radiation dose to personnel behind a shielding wall owing to their penetration capability. In addition to this, neutrons can generate activities through nuclear reaction, not only in accelerator devices, but also in materials surrounding the accelerator. The number of neutrons having energies from tens of MeV to several GeV is a primary concern since the capabilities of penetration and activation increase with energy, and, the neutron yield in the energy range is relatively high [1].

In the radiation safety design of high-energy accelerators, multiple particle transport codes are employed to describe particle generation and propagation under a finite geometrical condition [2–4]. The accuracy of the results obtained using the codes has been assessed using experimental data for an actual shielding condition. Until now, however, few data have been available for incident energies exceeding 100 GeV. Nakao et al. reported neutron energy spectra at several angles behind an iron and concrete wall for a 120-GeV/c mixed hadron beam on a 50-cm-long copper cylinder at the CERN–European Union High-Energy Reference Field (CERF) facility [5]. At the Fermi National Accelerator Laboratory (FNAL), neutrons were measured behind an iron and concrete wall using the unfolding technique of foil activation and Bonner spheres at an anti-proton production target facility for a 120-GeV proton beam [7–9]. Both CERF and FNAL results were compared with results calculated with theoretical codes, and systematic differences were observed.

To explain the differences observed in the shielding experiments, experimental data for the energy and angular distribution of neutrons with energies above tens of MeV, the so-called "source term", are required. Several experiments have been carried out to measure the source term in the GeV incident-energy range. The results for the source term have been used to develop and verify theoretical models [9]. Most source-term experiments, in contrast to shielding experiments, have the advantages of good energy resolution and freedom from an initial guess owing to the application of the time-of-flight (TOF) method. In the region above 10 GeV, however, only one dataset has been available. The data were recorded by Agosteo et al., who reported neutron spectra measured with Bonner spheres for a 40-GeV/c hadron (pion and proton) beam on 5-cm-thick copper at CERF in 2005 [10]. To obtain the neutron spectrum using Bonner spheres, the contribution made by the proton should be rejected according to theoretical calculation. The initial-guess neutron spectrum calculated theoretically is then indispensable in the unfolding process. There has been a demand for neutron spectrum data recorded employing the TOF technique, which has better energy resolution and does not rely on an initial guess in the region above 10 GeV to evaluate the source term.

To measure neutron energy employing the TOF technique, the time structure and uniformity of the beam should be prepared adequately. The time structure should have an adequate interval for the neutron flight time and data acquisition. Excellent beam uniformity helps greatly in finding a pair of beam and detector events. Unfortunately, the preparation of such a beam condition requires special hardware with unlimited beam adjustment for a synchrotron that provides a burst beam of high-energy particles with a fixed time interval. By considering the counting technique employed for the detector, the experiment can be carried out even under a nonuniform beam condition.

The Fermilab Test Beam Facility (FTBF) is a high-energy beam facility devoted to detector research and development for high-energy physics experiments [11]. At the FTBF, a 120-GeV proton or its secondary or tertiary particle (a several-GeV proton, pion, muon or electron) can be utilized with varying intensity using devices placed on the approximately 1500-m-long beam line. At the end of the beam line, there is a wide area to place a target and detectors. The facility is suitable for measuring the neutron spectrum while employing the TOF method, since the beam intensity can be reduced to perform pulse-by-pulse counting. This paper describes the methodology to measure the neutron spectra for the 120-GeV proton on a copper block using the TOF method at the FTBF. The obtained spectrum was compared with that obtained employing the conventional unfolding method and that deduced from the 40-GeV/c result to confirm the consistency of the experimental method.

2. Experimental

2-1. Facility and beam preparation

Experiments were carried out at the FTBF of the FNAL [11]. Figure 1 is a schematic diagram of the beam-preparation section of the facility. The facility has a beam line and equipment to utilize a 120-GeV proton from the main injector (MI) for the development and calibration of high-energy physics detectors. A 15.24-cm-long aluminum block was used as a beam diffuser. A pin-hole collimator (1 mm in diameter) with a tilting mechanism was used to adjust beam intensity. Particles passing through the collimator were analyzed on the basis of momentum using a series of magnets. The beam size and intensity were monitored using segmented ionization chambers and secondary-emission monitors installed in each section of the beam line.

Figure 2 shows a plan view of MT6 section 2 located at the end of the beam line. The area is an approximately 20 m × 10 m region enclosed by a concrete wall comprising blocks with cross sections of 90 cm × 90 cm and height of 270 cm and a thick iron beam dump. Users can lay out a target, detectors and beam-monitoring devices freely in this area to meet the requirements of their experiments. The height of the beam line is 167.5 cm from the floor level.

A copper block with a cross section of 5 cm × 5 cm and length of 60 cm was placed as a neutron production target on the beam line, 9 m downstream of the upstream wall of MT6 section 2. An array of 38 steel plates with thickness of 1.7 cm and spacing of 1.7 cm was placed 6.5 m downstream of the target. At 4.5 m downstream of the array, the thick iron dump of MT6 section 2 was installed permanently.

Figure 3 is a schematic diagram of the time structure of the FTBF beam. Up to 2×10^{11} 120-GeV protons were injected to the beam line in each spill. The spill had duration of 4 s every 1 min owing to the slow extraction of the MI. The time structure (train) of the spill had a fixed width ranging from 0.38 to 0.68 μs (depending on the beam mode) with 11-μs spacing in accordance with the revolution frequency of the MI. The train also had time structure (bunches) relating to the revolution frequency of the booster ring placed prior to the MI, the width of which was a few nanoseconds. The spacing of adjacent bunches was 19 ns. Thus, a single spill could provide a maximum of 3.64×10^5 trains and 1.31×10^7 bunches. Owing to the shielding structure of MT6 section 2 (especially the open top), the number of particle per spill was limited to keep the radiation level behind the shielding wall below FNAL regulations. The number of protons must be less than 3×10^5 per spill. The number of protons was controlled using

the aluminum block diffuser and the pin-hole collimator as shown in Fig. 1. The direction of the collimator was controlled by a tilting mechanism to reduce the beam intensity to the above value. Because the number of protons per spill (3×10^5) was comparable to the number of trains (3.64×10^5), each train had one proton on average, which means that single-proton counting could be performed in MT6 section 2 with sufficient time spacing for the neutron time-of-flight. In this procedure, the secondary particles produced at the diffuser and the collimator can be removed by a momentum separation section that follows the collimator.

The number of beam events (i.e., bunches with actual protons) in a train was measured as coincidence counts recorded by three thin plastic scintillators with photomultiplier tubes (beam monitors BM1, BM2, and BM3) placed on the beam line as shown in Fig. 2. BM1 had a cross section of 5 cm × 5 cm and thickness of 5 mm. BM2 and BM3 had the same cross section and were 1 mm thick. The raw signals (waveforms) obtained from photomultiplier tubes were recorded using a 10-bit fast digitizer (Agilent Acqiris DC282) with 0.5-ns sampling, 1-GHz bandwidth, and 500-ns duration for each coincidence count. The waveforms were analyzed to obtain the number of beam events in each waveform. Figure 4 shows the result. Fifty-five percent of trains contained a single beam event. The trains containing two or three beam events could be used by considering the time difference between the beam and detector events as described in a later section. The beam size on the Cu target was maintained at a full width at half maximum (FWHM) of around 5 mm by monitoring with two wire chambers (MT6WC1,2 in Figure 1) placed 13 and 23 m upstream of the target.

2-2. Detector and readout electronics

A cylindrical (12.7 cm in diameter by 12.7 cm in length) NE213 organic liquid

scintillator coupled with a photomultiplier tube (Hamamatsu R1250) was employed as a neutron detector because of its high detection efficiency, good timing resolution and neutron–gamma separation capability. An NE102A plastic scintillator (12.7 cm square and 5 mm thick) with a photomultiplier tube (Hamamatsu H1949) was placed as a veto detector immediately in front of the NE213 detector to tag charged particle events. The set of NE213 and veto detectors was placed 4.9 m from the target, at 90° with respect to the proton beam direction, at the same level as the beam height.

Figure 5 shows the data-acquisition electronics. The raw BM1, NE213 and veto signals were recorded as waveforms using the digitizer with 0.5-ns sampling and 1000 point data for each channel, event by event. The signal from the NE213 detector was divided into three by a signal divider (Div). One of the signals was fed to a constant-fraction discriminator (CFD; ORTEC935) to generate a trigger signal for the digitizer to record data with a low finite signal threshold, after coincidence with beam monitor signals. The other two signals were fed to the digitizer directory with different vertical full scales to enhance the resolution for the signal tail, which is important for neutron–photon separation. In addition to these two signals, signals from the veto and BM1 scintillators were fed to the digitizer directory. The waveforms for each trigger were stored in high-speed internal memory installed in the digitizer for up to 100 events. When the internal memory was filled up, the waveforms were automatically transferred to the main memory of a personal computer (PC) through a CompactPCI bus. After storing a few hundred events, the waveforms stored in the main memory were flushed to the hard disk drive of the PC during the beam-off period between spills (typically 56 seconds, see Fig. 3). Using this scheme, waveforms corresponding to about 90% of the NE213 triggers could be recorded by the PC. The remaining 10% of NE213 triggers had no waveform data since the data acquisition system was busy, and the corresponding

periods were treated as dead time. The effect of dead time was compensated for by taking the ratio of the number of NE213 triggers to the number of recorded waveforms. The numbers of beam events and NE213 triggers were counted using an external scalar for absolute normalization of the data.

3. Data analysis

3-1. Energy spectrum based on the TOF

The neutron spectrum, $d^2Y/dEdS$, can be computed as

$$\frac{d^2Y}{dEdS}(E) = \frac{C_n(E)\cdot f_{tof}\cdot f_{dead}}{(BM\cdot f_{multi})\cdot \varepsilon(E)\cdot S\cdot \Delta E}, \qquad (1)$$

where $C_n(E)$ is the energy spectrum obtained from the waveforms after choosing a non-charged particle, removing the photon event, choosing events exceeding the finite light output threshold, and choosing events for which the TOF can be determined without ambiguity. BM is the number of beam events counted as coincidence counts among three beam monitors during the measurement, $\varepsilon(E)$ is the detection efficiency of the NE213 detector, S is the area of the front surface of the NE213 detector, and ΔE is the energy bin width of the spectrum. In addition to these parameters, there are three correction factors in equation (1). f_{tof} is defined as the ratio of the total number of events to the number of events in which the TOF could be determined uniquely, f_{dead} is the ratio of the total number of triggers to the number of recorded waveforms, and f_{multi} is the average number of protons in a bunch.

f_{tof} was determined according to parameters, t_{tof} and the light output threshold, as described in the following. Figure 6 shows examples of NE213 and BM1 waveforms for events #44, #45, and #63, to explain how to determine f_{tof}. For event #44, the time

difference between NE213 and BM1, which was required for the TOF, could be determined uniquely because only one event could be seen in each waveform. In contrast to that event, event #45 had three beam events for a single NE213 event. It was clear that the No.3 event of event #45 was too late to be the beam event for NE213. Thus, No. 1 and No. 2 events were candidate beam events for the NE213 signal. In this case, we defined the parameter t_{tof} as the time period in which to accept a beam event, to decide the number of effective beam events. The end point of t_{tof} was determined as the arrival time of the fastest event, which is a proton-generated photon traveling from the target to the NE213 detector. As shown in the middle panel of Fig. 6, if t_{tof} was set to 80 ns, the TOF could be determined uniquely because the No. 1 event was out of range. If t_{tof} = 200 ns, the #45 event was discarded since the TOF cannot be determined uniquely. A shorter t_{tof} increases the number of events that determine the TOF uniquely; however, the energy dynamic range is reduced. Even for event #63, in which many protons are recorded within a waveform, the TOF can be determined uniquely if we employ t_{tof} =80 ns.

For several t_{tof} values, the integrals of the entire output signal of the NE213 detector and the tail components, and those of the veto and BM1 signals, the time difference between NE213 and BM1, and the number of events during t_{tof}, were computed from waveform data event-by-event to construct a data file for further analysis. The integrals of the NE213 waveforms were calibrated to the light output to obtain the "MeV electron equivalent (MeVee)" based on the Compton edges of ^{137}Cs and ^{60}Co radioactive gamma sources.

Figure 7 demonstrates the effect of employing single-event selection based on the number of events during t_{tof}. Both plots in the figure show the TOF versus light

output. The left and right plots are for all beam events and single-proton beam events with t_{tof} = 200 ns, respectively. The cyclic structure seen in the left plot originates from the bunch spacing (19 ns) of the beam. Once we choose a single beam event from the left plot, the structure completely disappears as shown in the right plot. Photon, neutron, pion, proton, and deuteron events are observed in the right plot.

Figure 8 presents f_{tof} values for three t_{tof} values as functions of the threshold light output. The greater t_{tof} value incurs the more discarded events owing to multiple beam events because the probability of a multiple beam event increases with the time period; thus, f_{tof} increases with t_{tof}. The f_{tof} value for each t_{tof} was determined by taking the average at higher light outputs, as shown by the dotted lines in Fig. 8, to avoid distortion due to incorrectly pairing TOF events as seen at lower light output. The TOF spectra multiplied with the f_{tof} value were identical; thus, the following analysis to obtain the final result was carried out with t_{tof} = 200 ns, which accepts the lowest light output threshold.

The numerical values for the other correction factors, f_{dead} and f_{multi}, were relatively small in comparison with the value of f_{tof}. f_{dead} is 1.11 as calculated from the scalar value of CFD pulses and the number of waveforms. f_{multi} is 1.15 as deduced from the pulse height distribution of the BM1 signal as shown in Fig. 9.

Figure 10 is a scatter plot of NE213 signals with the integrals of the entire and tail components for neutron–photon separation. The figure shows clear separation down to 2 MeVee. The light output threshold was set to 4.2 MeVee (AmBe bias) to obtain the time spectrum. The additional event discrimination between a charged particle and a non-charged particle was derived using the veto integral pulse height as shown in

Figure 11. Figures 12 and 13 are scatter plots of the TOF versus light output for non-charged and charged events, respectively. As shown in Fig. 12, there was a prompt photon peak prior to continuous neutron events. The FWHM of the prompt gamma peak was 1.62 ns, which mainly related to the flight time of a 120-GeV proton traveling the length of the copper target (60 cm). As shown in Fig. 13, proton events can be distinguished clearly from other events. Pion and deuteron events are also observed before and after proton events. Neutron events can be derived from the data in Fig. 12. The time spectrum for the neutron was converted to an energy spectrum according to the time difference from the gamma peak and flight path. The energy spectrum for the neutron was divided by the neutron detection efficiency $\varepsilon(E)$ of eq. (1), obtained using SCINFUL-QMD code [12]. The uncertainty in the efficiency of our detector system was estimated to be 15% on the basis of an examination using an intense white neutron source and 90-m flight path at LANSCE, Los Alamos National Laboratory [13]. The energy spectrum was normalized by the number of protons and the area of the front surface of the detector.

The errors taken into account for the neutron result were (1) statistical error (up to 10% below 140 MeV and up to 44% below 800 MeV) and (2) the detection efficiency (15% using SCINFUL-QMD code). The contributions from other errors, namely geometrical error, uncertainty in the number of protons and uncertainty in the correction factors, were relatively small in comparison with the contributions of the above two errors. The target out component was also negligible owing to the relatively long flight time for neutrons from the beam dump. The room-scattering component was not subtracted from the following result. It could be subtracted easily using data obtained in a separate run with a shadow bar, which is a thick iron block placed halfway between the target and detector to measure only the indirect portion.

3-2. Energy spectrum obtained using the unfolding method

To verify the result obtained in the above TOF data analysis with several correction factors, the neutron energy spectrum was deduced employing the conventional unfolding method. The unfolding method using the NE213 detector has been widely employed to deduce the neutron spectrum in shielding experiments when the TOF method is not applicable. The result obtained using the unfolding method is not affected by ambiguity of the TOF due to multi-proton events. Only data of the neutron pulse height and number of protons during the measurement are required to deduce the neutron energy spectrum.

The neutron pulse height data were obtained from waveform data by choosing non-charged particles, removing photon events, and choosing events exceeding a finite threshold light output, as described in the previous section. Note that multi-proton beam events were contained in the data. The pulse height signals were converted to the light output unit (MeVee) according to the calibration of not only the radioactive gamma sources but also the proton data. The procedure to obtain the proton data was as follows. (1) Proton events were identified using Fig. 13, (2) the energy of a proton was calculated from the TOF, and (3) the energy of a proton was converted to light output using data of Cecil code [14].

FORIST code [15] was used to deduce the neutron spectrum. A 30% window, which is one of the parameters to suppress fluctuations of the unfolded spectrum, was used for neutron energy groups above 20 MeV. The response matrix for the unfolding consisted of 18 neutron energy groups from 12 to 380 MeV. The response matrix was determined experimentally [16]. The uncertainty in the response matrix was estimated to be 15%.

4. Results and discussions

Figure 14 shows the measured neutron energy spectra obtained using the TOF and unfolding method at 90 degrees for the 120-GeV proton on a 60-cm-long copper target. In addition, the neutron spectrum at a distance of 60 cm and an angle of 90 degrees for 40-GeV/c hadrons (25% protons and 75% pions) on a copper target with diameter of 2 cm and length of 5 cm is also presented (obtained with Bonner spheres by Agosteo et al. [10]), the magnitude of which was normalized to compensate for the difference in experimental conditions. Table 1 summarizes the normalization factors used for the data of Agosteo et al. The difference in incident energy was compensated for using the empirical equation of the neutron yield:

$$Y_n \propto E^{0.8}, \qquad (2)$$

where Y_n is the neutron yield and E is the energy of the incident particle [1]. The resultant factor was 2.41. The neutron yield of the pion was estimated using PHITS code [2] to be approximately 1.6 times less than that of the proton having the same energy. The effect of the distance between the target and detector was compensated for using the inverse r^2 law, giving a normalization factor of 0.015. The geometrical difference was compensated for in both the longitudinal and transversal directions using the interaction length, λ_I:

$$\lambda_I = 37.8 \cdot A^{0.312}, \qquad (3)$$

where A is the mass number of the media (Z > 15) [1]. Normalization factors of 3.5 and 2.38 were obtained for longitudinal and transversal directions, respectively.

As shown in Fig. 14, the neutron spectrum obtained from the TOF is in good agreement with that obtained by unfolding within the margin of error. This indicates the relevance of the correction factors, especially f_{tof}, used in the data analysis of the

TOF method. It is important to note the difference in the energy ranges covered by the two methods. The energy range of the unfolding method is limited by the lack of a response matrix because it is difficult to obtain the matrix for the high-energy region experimentally. On the other hand, the upper energy of the TOF method is limited by the timing resolution of detectors and the geometry since the time difference between the neutron and photon becomes smaller than the resolution. The timing resolution can be estimated from the prompt-photon peak time width of 1.62 ns for the present setup. The timing resolution determines the energy resolution as a function of neutron energy: a maximum of 44% for 800 MeV and a minimum of 4% for 20 MeV. The resolution could be improved by reducing the target length, since a relatively long target length (60 cm) produces a large time spread, 1 ns on average. By reducing this thickness while considering the neutron yield, the energy range to be measured from the TOF is sufficient to cover a few GeV, which can provide information on the neutron effect in the radiation safety design of a high-energy accelerator. The largest error sources in experimental results other than the statistics are the detection efficiency and response function for the TOF and unfolding methods, respectively. Improvement of the detection efficiency to reduce error experimentally would be easier than improving the response function. Above the applicable energy limit of the TOF method, only the calorimetric method could be used to obtain the neutron spectrum.

The present results are also consistent with data obtained using a Bonner sphere for a 40-GeV/c hadron beam on thin copper [10] in the energy region from 100 to 400 MeV. Below 100 MeV, the present data would be affected by floor scattering that can increase results because of the longer distance from the target to the detector. Above 400 MeV, employing a Bonner sphere faces the difficulty of a relatively strong response to charged hadrons (protons and positive and negative pions). Moreover, it

would be difficult to change the Bonner sphere response in this energy range. The Bonner sphere requires calculation results for the initial guess of the unfolding process and the rejection of charged-particle events. In contrast, the TOF method can determine the neutron spectrum without any initial guess, and easily rejects charged-particle events according to the veto pulse height (Fig. 10). In addition to this, the charged-particle spectra could be deduced from data (Fig. 12), and they would be useful benchmark data for theoretical codes since the detection efficiency is more reliable than that for the neutron.

5. Conclusion

A methodology to measure the neutron energy spectrum was established at the FTBF of FNAL. The 120-GeV proton beam was prepared for event-by-event counting of primary and secondary particles to allow TOF energy determination. An NE213 organic liquid scintillator with a veto plastic scintillator and a pulse-shape discrimination technique were employed to identify neutrons. Raw waveforms of the beam and veto and NE213 scintillators were recorded to remove effects from multi-proton beam events. The neutron energy spectrum ranging from 10 to 800 MeV was obtained for a 60-cm-long copper target at 90 degrees to the beam axis. The resultant spectrum was consistent with that deduced by conventional unfolding and that obtained in a 40-GeV/c thin-target experiment. As a result, we can receive the full benefit of the TOF method for measurement in the incident energy region above tens of GeV since the FTBF beam line can provide a variety of energies and particle beams in the same manner.

The apparatus could be applied directly to the measurement of double differential cross sections (DDXs) for neutron and charged-particle production, which

can evaluate theoretical models implemented in a multi-particle transport code. The set of DDXs at several angles for various materials allows systematic comparison between the results of experiment and calculation, as has been done in the low-energy region. To obtain the DDX, subtraction of the room-scattering components should be considered. Obtaining these data is the next step of this study.

Acknowledgments

This work is supported by a grant-in-aid from the Ministry of Education (KAKENHI 20357464) of Japan. Fermilab is a U.S. Department of Energy Laboratory operated under contract DE-AC02-07CH11359 by the Fermi Research Alliance, LLC.

References

[1] Particle data group, Review of particle physics, *Journal Physics* **G37**, 7A (2010) 075021

[2] N.V.Mokhov, "The MARS Code System User's Guide", Fermilab-FN-628(1995); N.V.Mokhov, S.I.Striganov, "MARS15 Overview", in Proc. Hadoronic Shower Simulation Workshop, Fermilab, September 2006, AIP Conf. Proc. 896 50 (2007)

[3] K.Niita et al., "PHITS: Particle and Heavy Ion Transport code System, Version 2.23", *JAEA-Data/Code* 2010-022 (2010)

[4] A.Fassò et al., "FLUKA: a multi-particle transport code", CERN-2005-10 (2005), INFN/TC_05/11, SLAC-R-773

[5] N.Nakao, et al, *Nucl. Instrum. Meth.* **B266** (2008) 93-106

[6] H.Nakashima et al., *"JASMIN: Japanese-American Study of Muon Interactions and Neutron detection", Proceedings of 10th workshop of Shielding Aspects of Accelerators, Targets and irradiation facilities", CERN, Switzerland, 2-4 June 2010, in press*

[7] Y. Kasugai, et al., *"Shielding Experiments under JASMIN Collaboration at FERMILAB (I) Overview of the Research Activities", J Korean Phys Soc, 59[No. 2], 2063-2066 (2011).*

[8] M.Hagiwara et al., *"Shielding Experiments at High Energy Accelerators of Fermilab (III):Neutron Spectrum Measurements in Intense Pulsed Neutron Fields of The 120-GeV Proton Facility Using A Current Bonner Sphere Technique" Progress in Nuclear Science and Technology, 1 52-56 (2011).*

[9] K.Ishibashi et al, *J.Nucl.Sci. Technol.* **34** (1997) 529-537

[10] S.Agosteo et al., *Nucl.Instrm.Meth.* **B229** (2005) 24-34

[11] http://www-ppd.fnal.gov/MTBF-w/

[12] D.Satoh et al., "SCINFUL-QMD: Monte Carlo based computer code to calculate response function and detection efficiency of a liquid organic scintillator for neutron energies up to 3 GeV", *JAEA-Data/Code* 2006-023 (2006)

[13] N.Shigyo et al., *"Neutron energy spectrum from 120 GeV protons on a thick copper target", Proceedings of 10th workshop of Shielding Aspects of Accelerators, Targets and irradiation facilities", CERN, Switzerland, 2-4 June 2010, in press*

[14] R.A.Cecil et al., *Nucl.Instrm.Meth.* **161** (1979) 439-447

[15] R.H.Johnson, FORIST, Neutron spectrum unfolding code (FERDOR with optimized resolution using an iteractive smoothing technique), PSR-92, RSIC/ORNL, 1976.

[16] S.Taniguchi et al, *Nucl. Instrm. Meth.* **A 562**, 2006, 954

Table title

Table 1 Numerical values for normalization factors of the neutron spectrum obtained by Agosteo et al.

Figure captions

Fig. 1. Schematic diagram of the beam preparation section of the FTBF.

Fig. 2. Plan view of MT6 section 2 with beam monitors (BMs), a Cu target and an NE213 organic liquid scintillator, as well as shielding walls and a beam dump.

Fig. 3. Schematic view of the FTBF beam time structure for MT6-section 2.

Fig. 4. Number of events in beam triggers per train.

Fig. 5. Schematic diagram of data acquisition electronics. TGT: Target, BM: Beam monitor, nsD: nano second Delay, Div: signal Divider, CFD: Constant Fraction Discriminator, COIN: Coincidence, DC282: Acqiris Digitizer.

Fig. 6. Example of NE213 and BM1 waveforms for events #44 (top panel), #45 (middle panel) and #63 (bottom panel). The TOF can be computed if the time difference between NE213 and the beam monitor is determined uniquely (#44 case). In event #45, the TOF is also determined if we choose t_{tof} = 80 ns, which is an acceptable duration for the beam-monitor signal. t_{tof} = 80 ns is also acceptable for event #63. Event #45 is discarded

if t_{tof} = 200 ns is chosen. The number of discarded events is corrected for using f_{tof} (see text).

Fig. 7. Demonstration of the effect of single-event selection. Both plots show the TOF versus light output; however, the left and right plots are respectively for all events and single-proton beam events with t_{tof} = 200 ns. The cyclic structure seen in the left figure originates from the bunch spacing (19 ns) of the beam. The cyclic structure completely disappears by choosing only a single beam event. Photon, neutron, pion, proton, and deuteron events can be distinguished in the right plot.

Fig. 8. f_{tof} values for three t_{tof} values as functions of the threshold light output. A longer t_{tof} value results in more events being discarded owing to multi-proton beam events. f_{tof} increases with t_{tof}. The f_{tof} value for each t_{tof} was determined by taking average value at relatively high light outputs to avoid distortion due to incorrect TOF events at lower light output.

Fig. 9. Pulse height distribution of the beam-monitor scintillator (BM1)

Fig. 10. Scatter plot of neutron–gamma separation for neutral particles

Fig.11. Scatter plot of veto–total light output

Fig. 12. Scatter plot of TOF–light output for non-charged events

Fig. 13. Scatter plot of TOF–light output for charged events

Fig. 14. Measured neutron energy spectra obtained using the TOF (closed circles) and unfolding method (open squares) at 90 degrees for a 120-GeV proton on a 60-cm-long copper target. The solid line shows the experimental result obtained by Agosteo et al. using Bonner spheres. The Bonner sphere data were normalized to compensate for the difference in experimental conditions as described in Table 1.

Table1 Numerical values for normalization factors of neutron spectrum obtained by Agosteo et al.

Item	Present	Agosteo et al [9]	Method	Normalization factor
Energy	120 GeV	40 GeV/c	Neutron production rate	2.41
Beam particle	proton	25% proton 75% pion	Neutron production rate	1.6
Distance	495 cm	60 cm	Inverse r^2 law	0.015
Target length	60 cm	5 cm	Interaction length	3.5
Target cross section	5x5 cm (effective diameter 5.6cm)	2cm	Interaction length	2.38

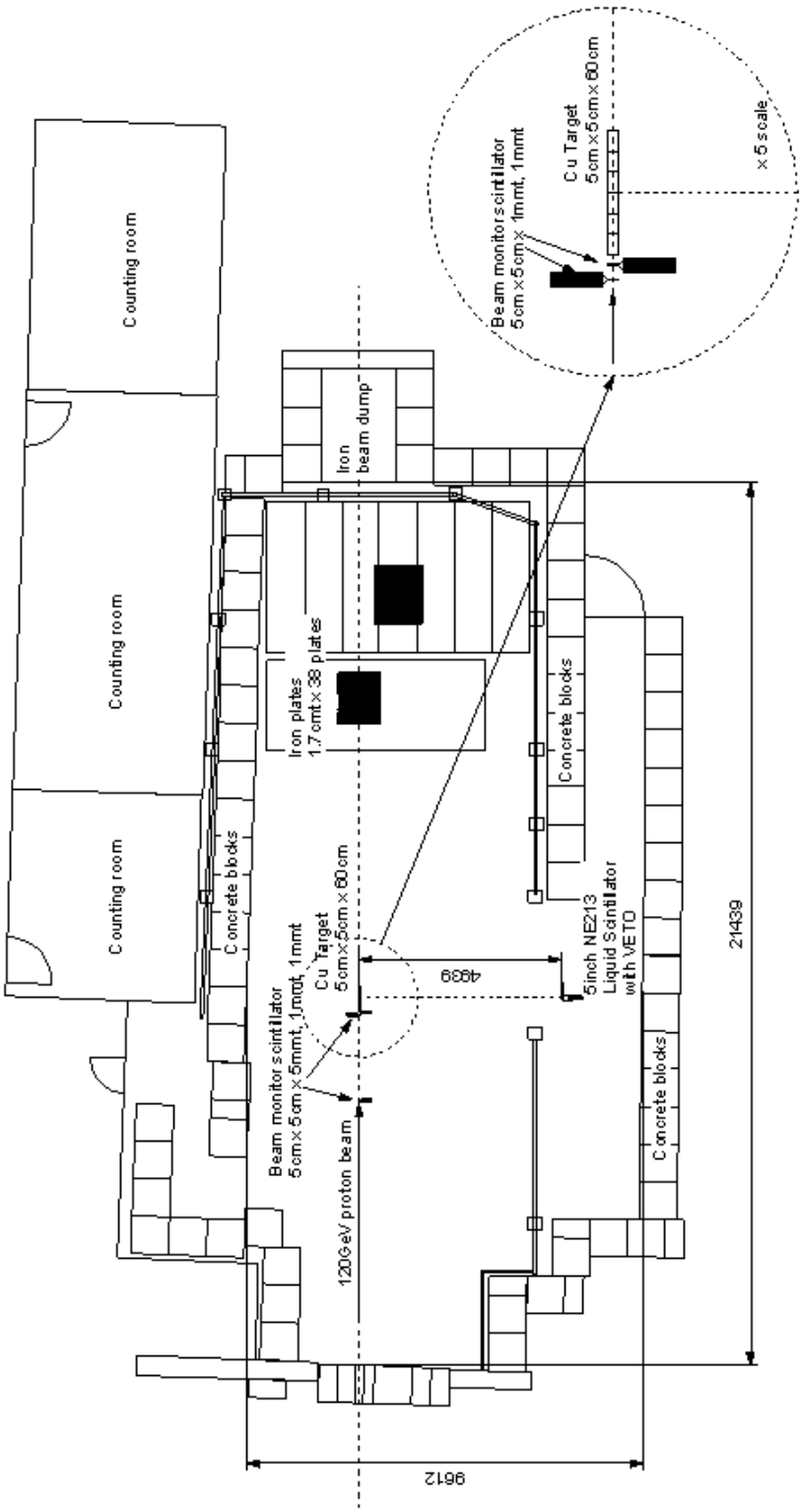

Fig. 2. Plan view of MT6 section 2 area with beam monitors (BMs), Cu target and NE213 organic liquid scintillator, as well as shielding walls and a beam dump.

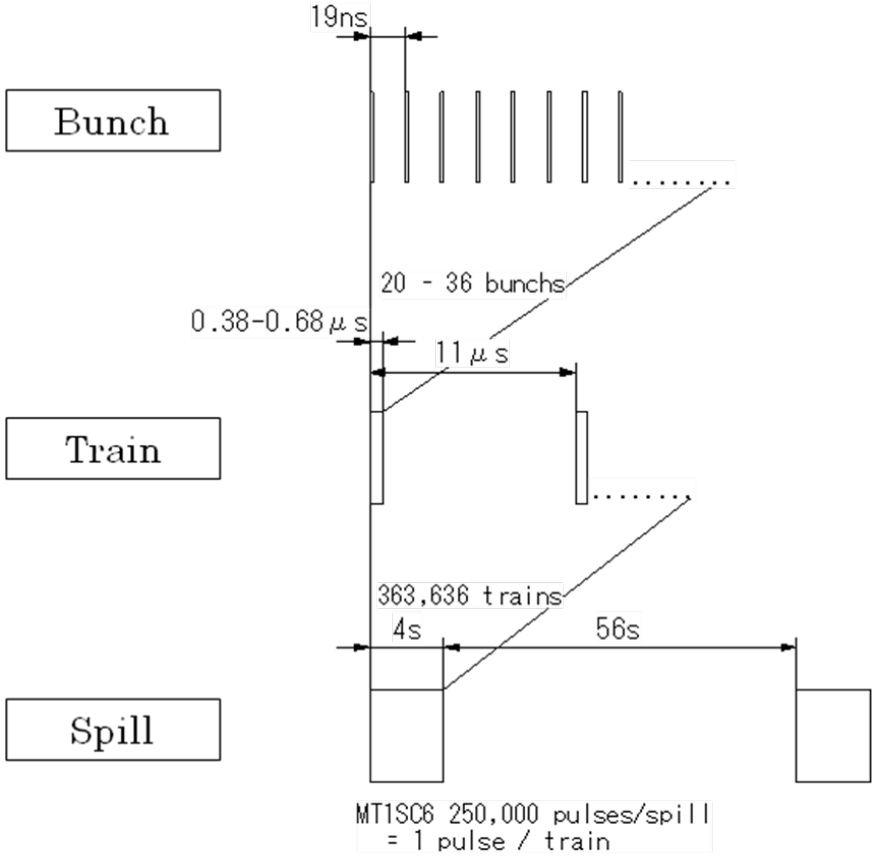

Fig. 3. Schematic view of FTBF beam time structure for MT6-section2 area

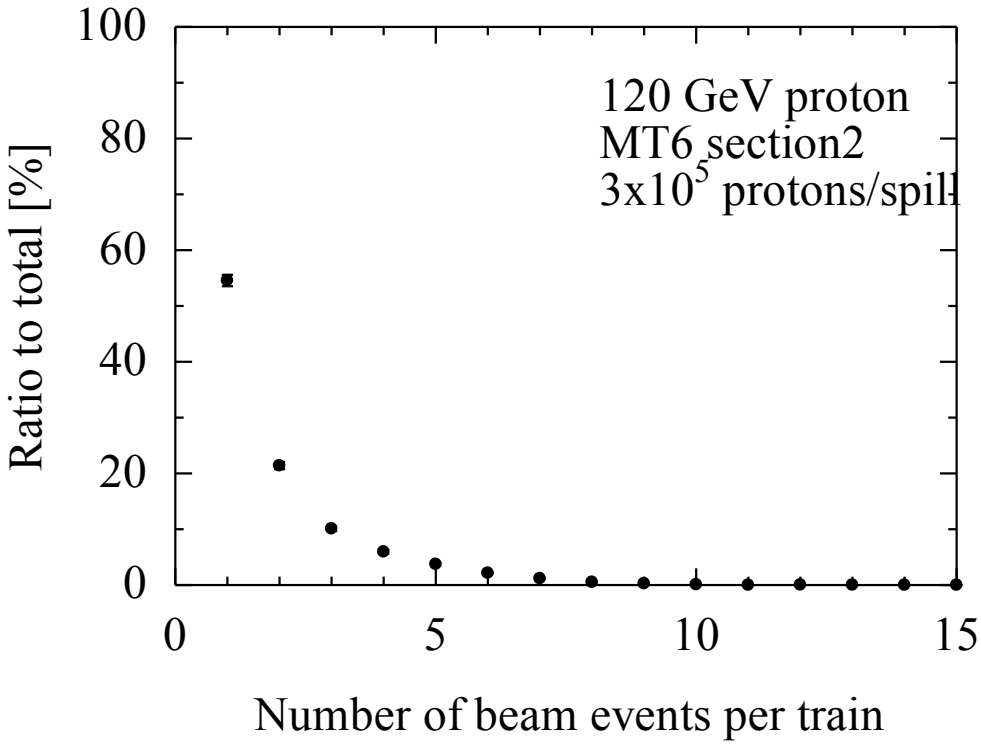

Fig. 4. Number of events on beam triggers per train

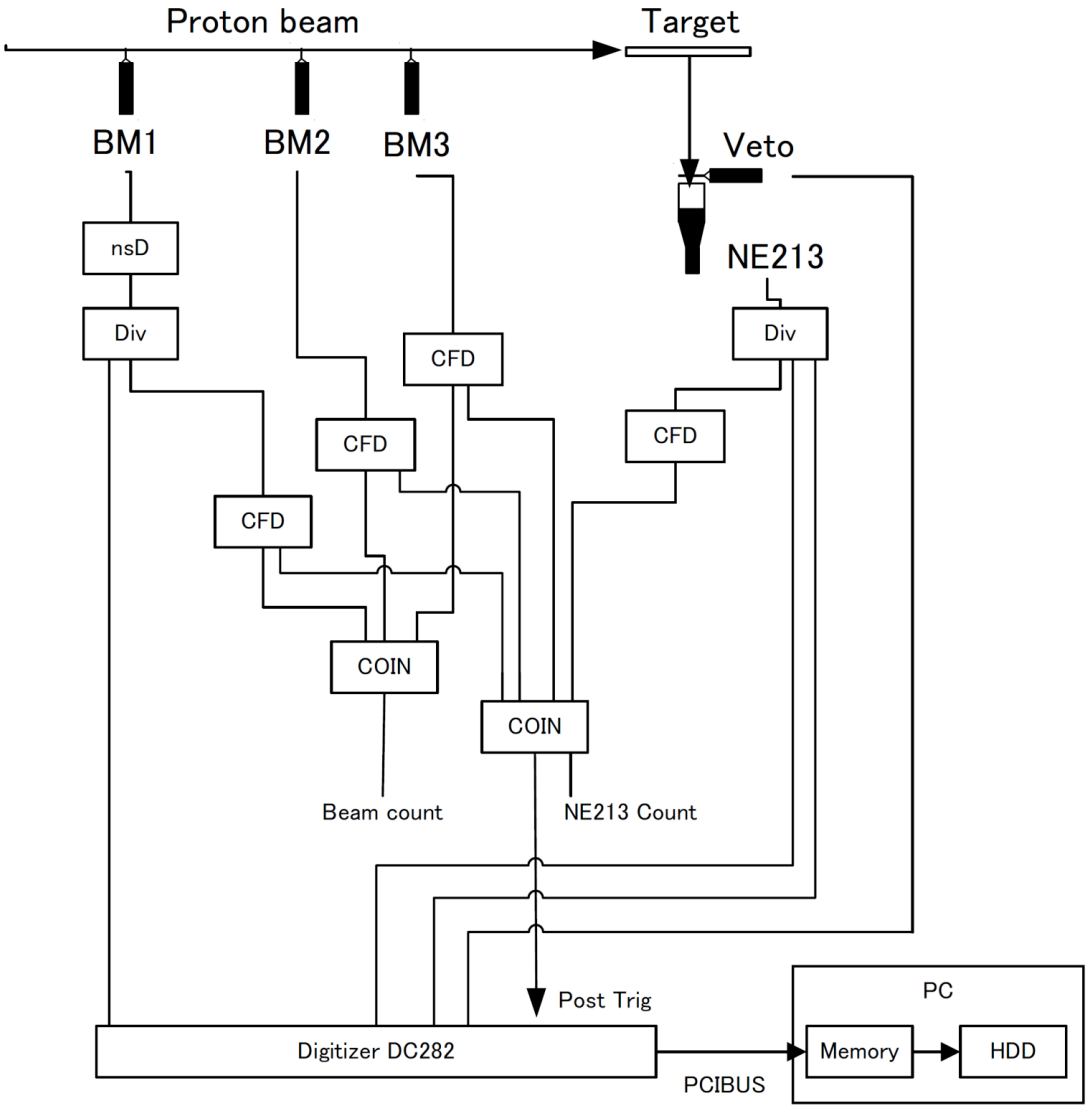

Fig. 5. Schematic diagram of data acquisition electronics. TGT: Target, BM : Beam monitor, nsD : nano second Delay, Div : signal Divider, CFD : Constant Fraction Discriminator, COIN : Coincidence, DC282 : Acquris Digitizer

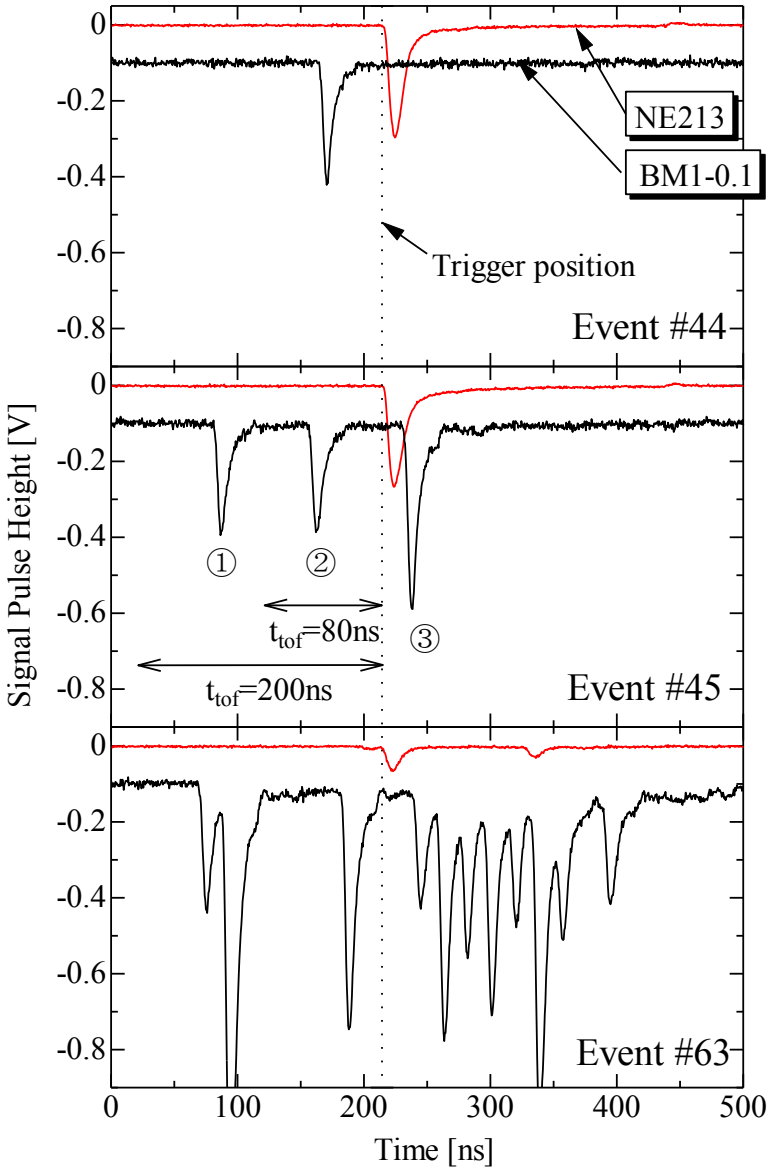

Fig. 6. Example of NE213 and BM1 waveforms for event #44(top panel), #45(middle panel) and #63(bottom panel). TOF can be computed if time difference between NE213 and BM is determined uniquely (#44 case). #45 case also determined TOF, if we choose t_{tof} =80 ns, acceptable duration for BM signal. #63 event is also valid for t_{tof} =80 ns. #45 event is discarded if t_{tof} =200 ns is chosen. The number of discarded events is corrected using f_{tof} (see text).

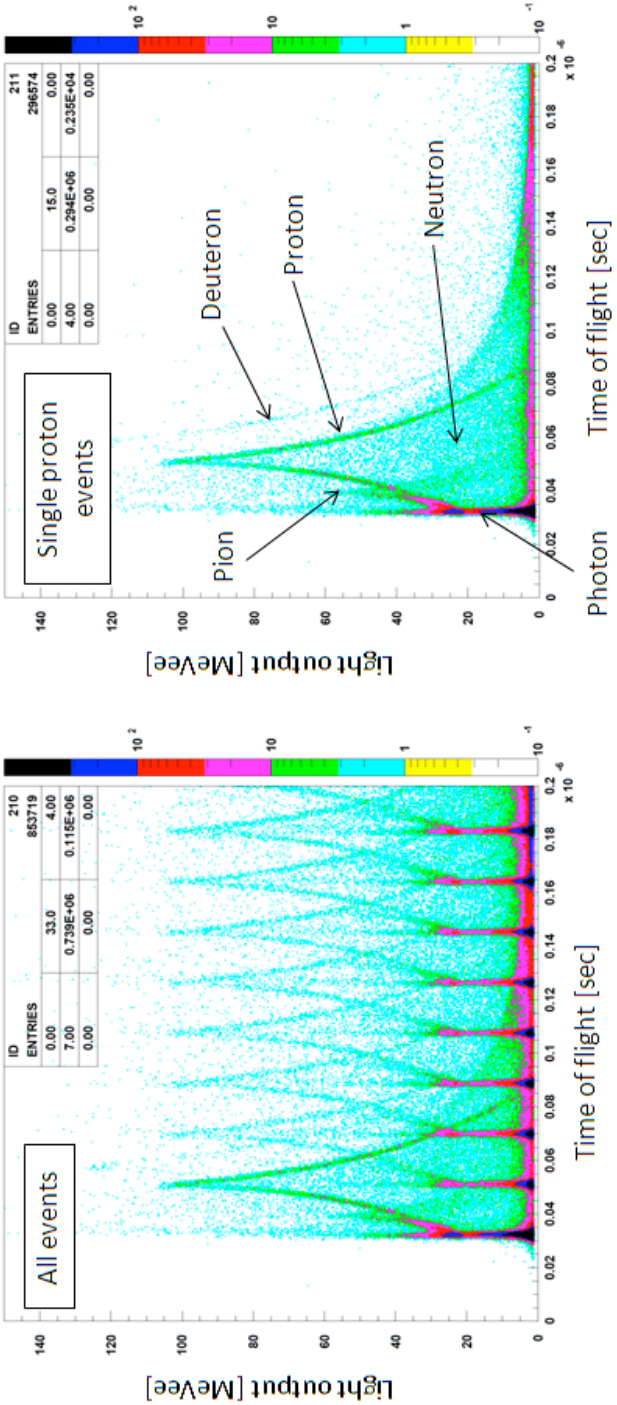

Fig. 7. Demonstration for effect of single event selection. The both plots show TOF vs light output, however, the left and right plot are for all and single beam event with t_{tof} =200ns. The cyclic structure seen in the left figure is originated from bunch spacing (19ns) of the beam. The cyclic structure is completely disappeared by choosing only single beam event. Photon, neutron, pion, proton, and deuteron events can be distinguished on the right plot.

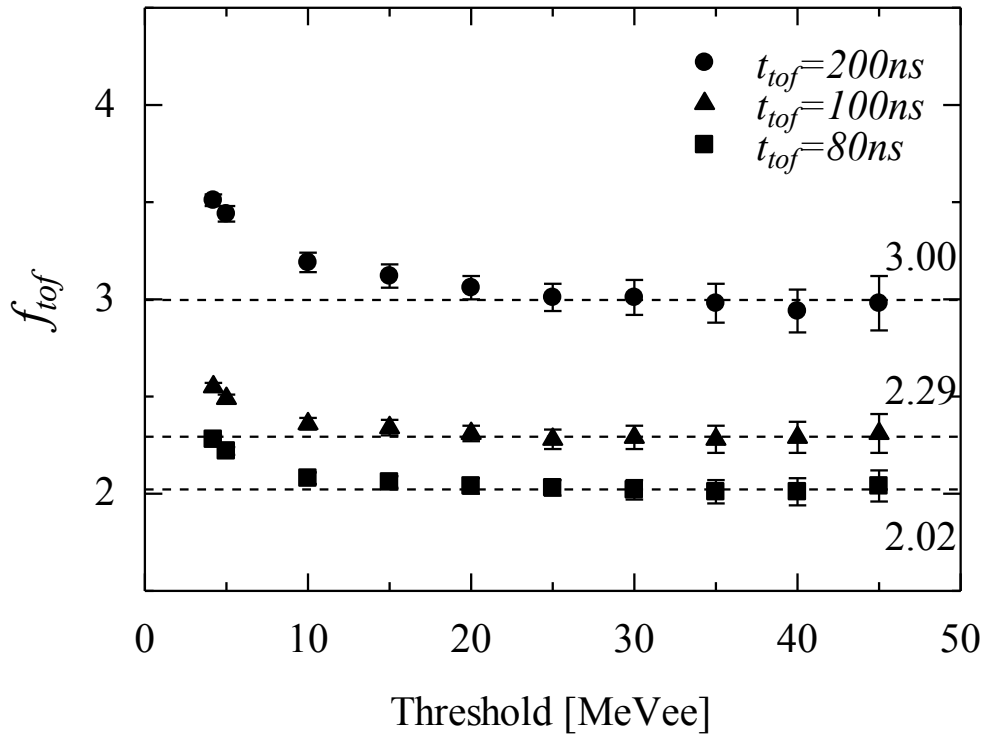

Fig. 8. f_{tof} values for three t_{tof} values as a function of threshold light output. The longer t_{tof} value incur more event discarded owing to multi beam event. f_{tof} value becomes higher with t_{tof}. The f_{tof} value for each t_{tof} was determined by taking average of f_{tof} values with relatively higher light output to avoid distortion due to wrong TOF events that could be seen in lower light output event.

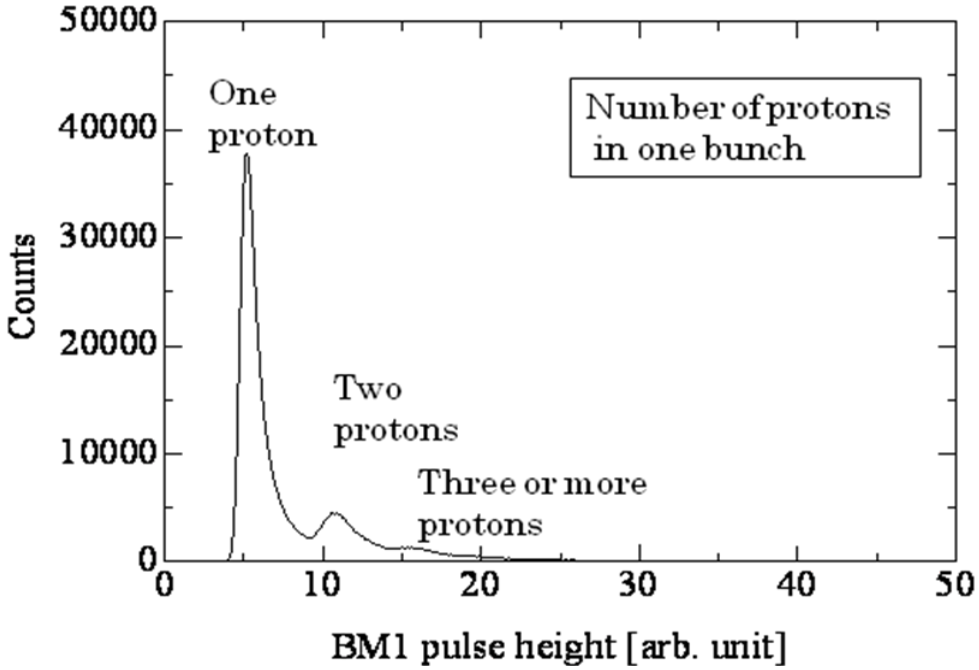

Fig. 9. Pulse height distribution of beam monitor scintillator (BM1)

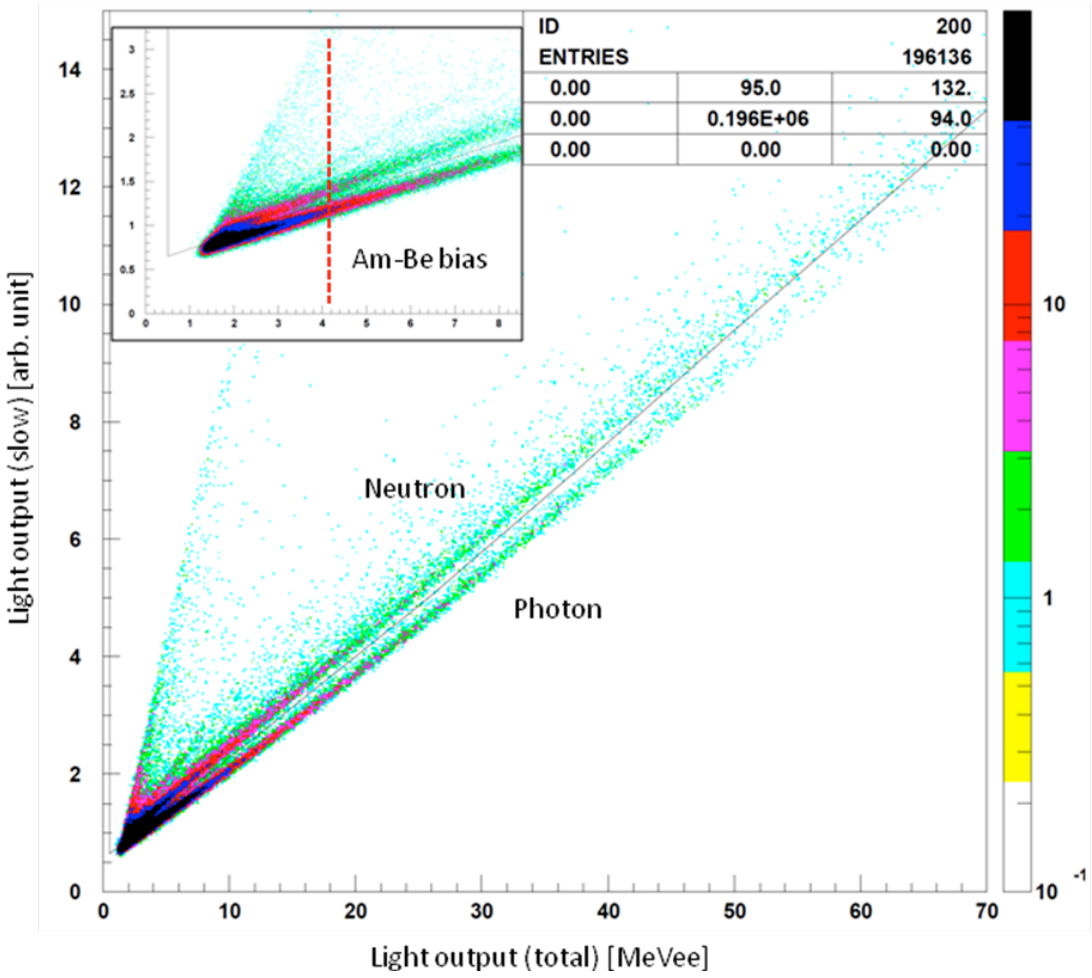

Fig. 10. Scatter plot of neutron-gamma separation for neutral particles

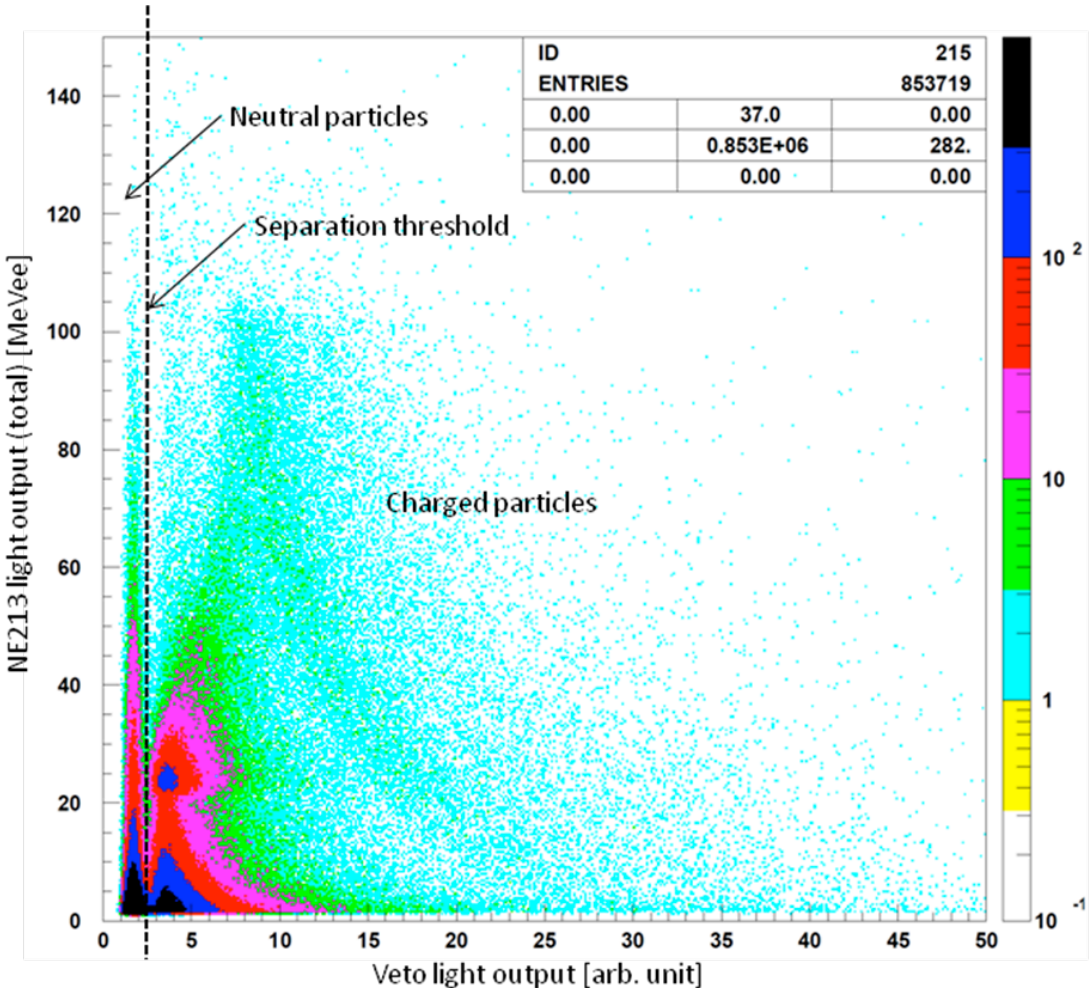

Fig. 11. Scatter plot of Veto – total light output

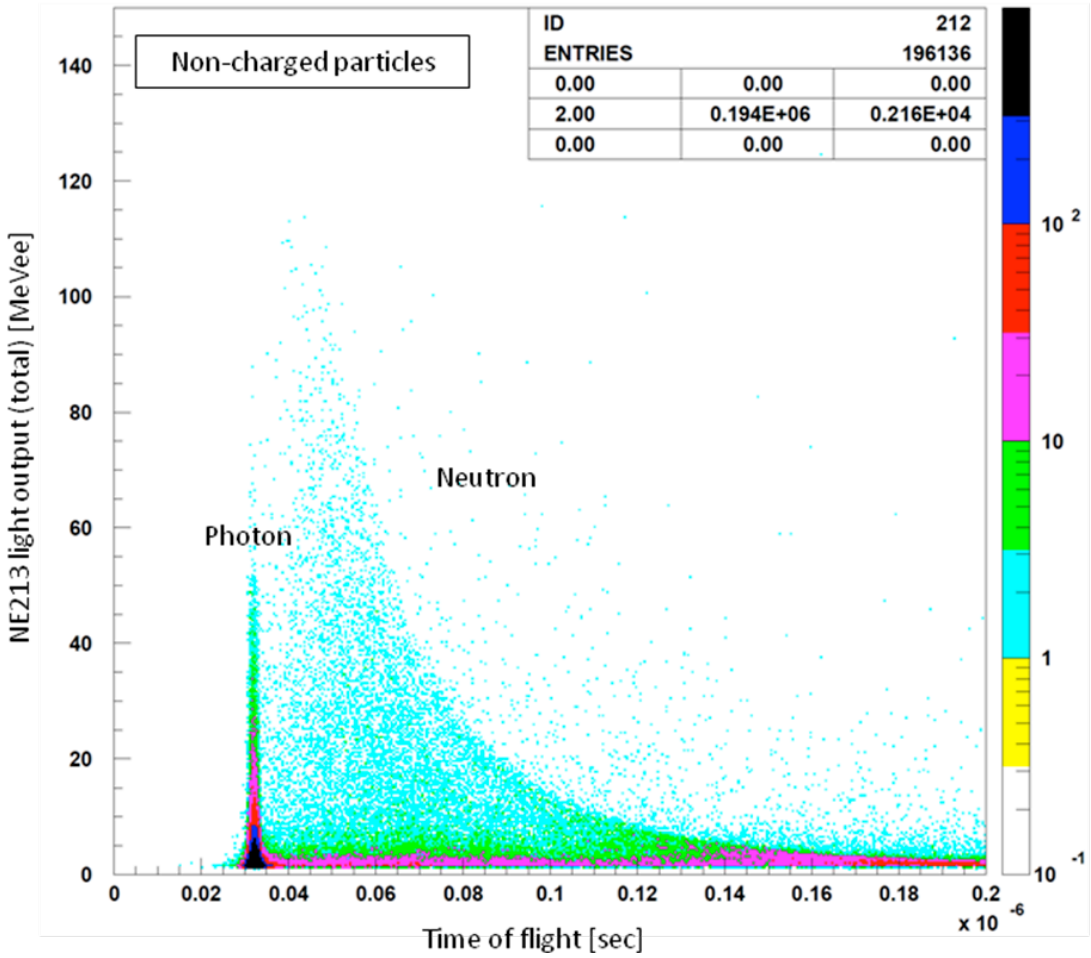

Fig. 12. Scatter plot of TOF-light output for non-charged events

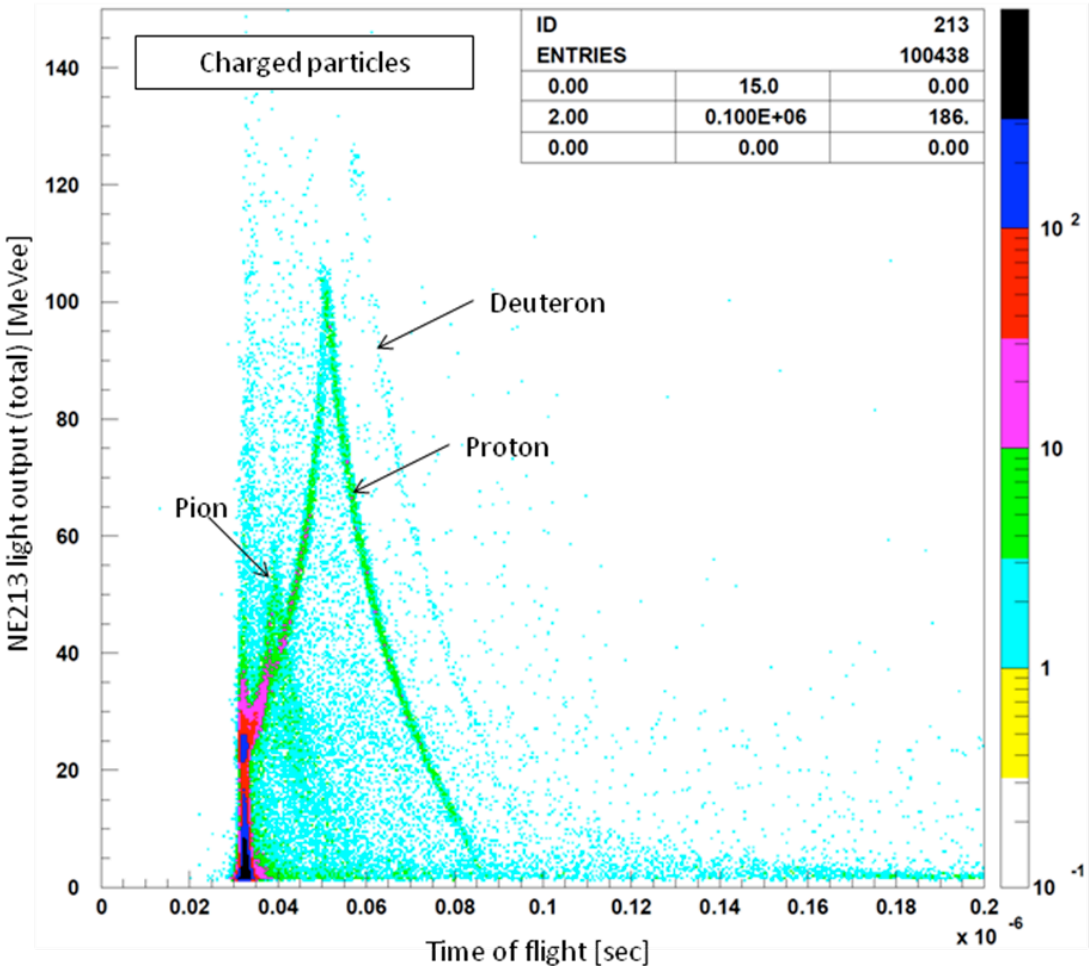

Fig. 13. Scatter plot of TOF-light output for charged events

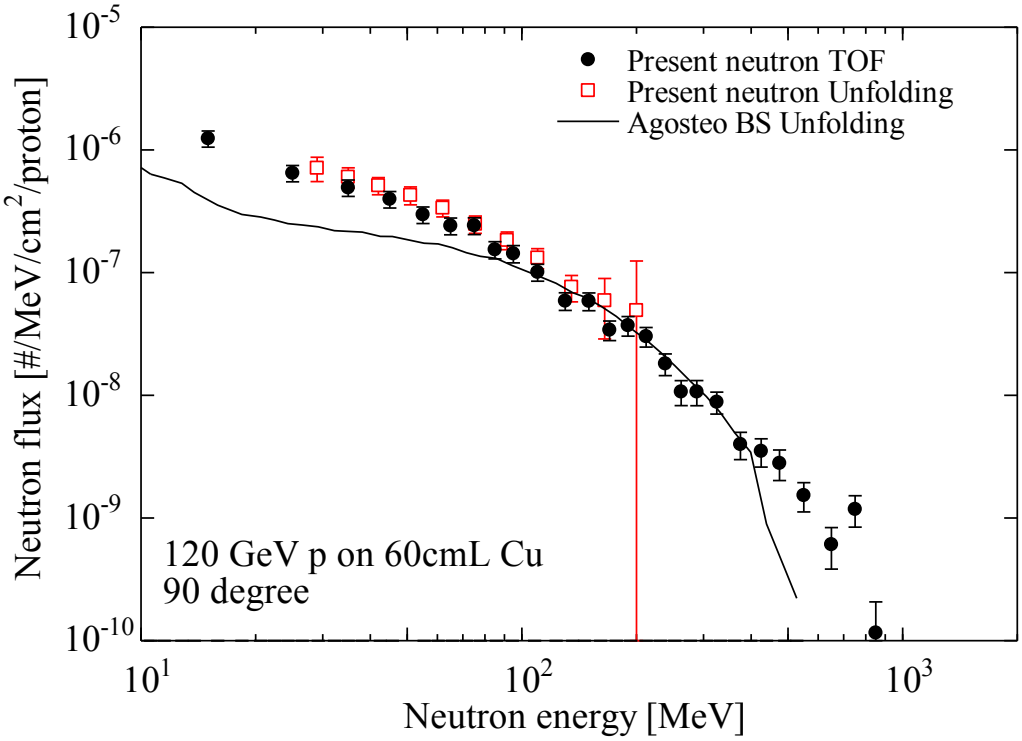

Fig. 14. Measured neutron energy spectra obtained by TOF (closed circles) and unfolding method (open squares) at 90 degrees for 120 GeV proton on a 60 cm long copper target. Solid line shows experimental result taken by Agosteo et al using Bonner spheres. The magnitude of Agosteo BS data was normalized to compensate difference of experimental conditions as listed in Table 1.